Observations of the 86 GHz SiO maser sources in the Central Parsec of the Galactic Centre

Borkar, A.[1]*, **Eckart, A.**[2,3], **Straubmeier, C.**[2], **Sabha, N. B.**[2], **Sjouwerman, L. O.**[4], **Karas, V.**[1], **Kunneriath, D.**[5,1], **Moser, L.**[4,2], **Britzen, S.**[3], **Valencia-S, M.**[2], **Donea, A.**[7], **Zensus, A.**[3,2]

[1] *Astronomical Institute of the Academy of Sciences, Prague, Boční II 1401/1a, CZ-14131 Praha 4, Czech Republic*

[2] *I. Physikalisches Institut, Universität zu Köln, Zülpicher Strasse 77, D-50937, Köln, Germany*

[3] *Max-Planck-Institute für Radioastronomie, Auf Dem Hügel 69, D-53121, Bonn, Germany*

[4] *National Radio Astronomy Observatory, PO Box 0, Socorro, NM 87801, USA*

[5] *National Radio Astronomy Observatory, 520 Edgemont Road, Charlottesville, VA 22903, USA*

[6] *Argelander-Institut für Astronomie, University of Bonn, Auf dem Hügel 71, D-53121 Bonn, Germany*

[7] *Monash Centre for Astrophysics, Monash University, Clayton, Victoria 3800, Australia*

We present results of 3 mm observations of SiO maser sources in the Galactic Centre (GC) from observations with the Australia Telescope Compact Array between $2010-2014$, along the transitions of the SiO molecule at $v = 1, J = 2-1$ at 86.243 GHz and $v = 2, J = 2-1$ at 85.640 GHz. We also present the results of the 3 mm observations with Atacama Large Millimeter/Submillimeter Array (ALMA). We detected 5 maser sources from the ATCA data, IRS 7, IRS 9, IRS 10EE, IRS 12N, and IRS 28; and 20 sources from the ALMA data including 4 new sources. These sources are predominantly late-type giants or emission line stars with strong circumstellar maser emission. We analyse these sources and calculate their proper motions. We also study the variability of the maser emission. IRS 7, IRS 12N and IRS 28 exhibit long period variability of the order of $1-2$ years, while other sources show steady increase or decrease in flux density and irregular variability over observation timescales. This behaviour is consistent with the previous observations.

---

*Speaker; E-mail: borkar@asu.cas.cz

1. Introduction

The innermost parsec of the Milky Way is a complex environment (hereafter referred to as the central parsec), with a supermassive black hole (SMBH) of mass of $4 \times 10^6 M_\odot$ at the centre. The SMBH is associated with the compact radio source, Sagittarius A* (Sgr A*) located at a distance of 8 kpc (see, e.g. [1, 2, 3, 4, 5] for detailed review of the topic). The central parsec consists of an extremely dense collection of stars as well as 'the mini-spiral' of filaments of ionized gas, and it is surrounded by a circumnuclear disk (CND) of neutral atomic & molecular gas at $\simeq 1.5$ pc that extends upto $\sim 5 - 7$ pc. Observations of the central stellar cluster have discovered a large population of mainly late-type red giant stars, including asymptotic giant branch (AGB) stars (*see e.g.* [6, 7, 8, 9, 10]). Spectroscopic observations have found hot, early-type stars with H, He, and N emission lines showing characteristics of post main-sequence Ofpe/WN9, luminous blue variables (LBVs) and Wolf-Rayet stars [11, 12, 13, 7, 14, 8].

Recent observations have also discovered several massive young stellar objects (YSOs) ($\sim 10 - 120\ M_\odot$, age $\lesssim 10 - 100$ Myr). These include more than 100 main-sequence OB stars, luminous OB giants and supergiants, post main-sequence Wolf-Rayet stars, and Herbig Ae/Be stars in the central parsec, as well as the S-star cluster of > 15 main-sequence B stars within $1''$ (0.04 pc), very close to the SMBH [15, 16, 17, 18, 19, 20, 21, 22, 8, 23, 24, 25, 12, 26, 27, 28]. The presence of such young stars so close to the black hole is perplexing, and has been a hotly debated issue, sparking several dynamical models. These models are mainly categorised into two groups: (1) in-fall, or dynamical migration of the stellar cluster from outer zone ([29, 30, 31] and references therein) and (2) *in-situ* star formation ([32, 33] and references therein). Analysis of the population of young stars in the central parsec suggests an age of $\sim 4 - 8$ Myr. The presence of two similar young (age $2 - 7$ Myr), massive ($\sim\ 10^4 M_\odot$) star clusters with similar stellar population, the Arches and the Quintuplet, within 50 pc of the Galactic Centre (GC) alludes to the possibility of a global event a few million years ago that could have led to the star formation in the GC [34, 8, 35]. To understand the origins of the stars in the central parsec, observations of their spatial distribution in different frequency bands are required.

The central stellar cluster contains stars which are bright infrared (IR) sources and strong sources from the SiO maser emission. The SiO maser emission arises from the rotational transitions within the vibrational states of the SiO molecule, and is mainly associated with late-type red giant stars, especially AGB stars and planetary nebulae [36, 37, 38, 39, 40, 41]. SiO maser emission has been observed in massive young stellar objects, but it is very rare [42, 43, 44, 45]. The radiative pumping from the IR radiation and collisional pumping are thought to be the mechanisms responsible for the SiO maser emission from the stellar atmosphere [40]. Very long baseline interferometry (VLBI) observations have shown that SiO masers originate in the circumstellar envelope of the star, at a distance of $\sim 10^{14}$ cm, closer than the OH & H_2O masers, which are found further out in the stellar atmosphere [38]. The SiO emission arises from cells close to the star, which describes the stellar position within 1 mas and can be treated as point sources [42, 46]. Stellar objects with SiO maser emission act as reliable tracers for Galactic dynamics as they are not sensitive to non-gravitational perturbations [47, 48].

Since these sources are strongly visible in both the radio line emission and the IR, their radio positions have been used to create a reference frame to perform accurate astrometry for the IR images which was used to locate the precise position of Sgr A* in IR [49, 50, 51]. The central parsec has been observed extensively for SiO sources at 43 GHz line at high resolution with the Very Large Array (VLA), the Very Long Baseline Array (VLBA), and the Australia Telescope Compact Array (ATCA) [49, 52, 53, 54, 55, 56, 47, 57, 58, 50, 51, 59, 48, 24]. Comparatively, the 86 GHz SiO line sources are still largely unexplored. [60] and [61] observed the inner Galaxy using single dish telescopes, i.e. Nobeyama 45 m telescope and IRAM 30 m telescope respectively, but their observations were limited by angular resolution and sensitivity. Interferometric observations at 86 GHz were performed by [48] using ATCA in 2006 and 2008. Their observations were limited by the velocity coverage ($\pm 30 - 60$ km s^{-1}), where they detected two sources: IRS 10EE and IRS 15NE. Further observations by Li et al. also detected IRS 7, IRS 10EE, IRS 12N, IRS 15NE, IRS 17, IRS 28, SiO 15 and SiO 20 (J. Li, L. O. Sjouwerman & C. Straubmeier, private communication). A census of the stellar sources in the central parsec at different wavelengths is necessary to understand the physical processes that govern the stellar distribution in the GC.

In this paper, we report the results of our observations of the GC environment at 3 mm, taken between 2010 to 2014 using the ATCA, and publicly available data from ALMA observation in 2015. In Section 2, we describe the observations and data reduction processes used to obtain the positions of the detected maser sources. The results of the observations are discussed in Section 3, where we report proper motions of the stars. The analysis of the detected maser sources and their observed variability is discussed in Section 4, followed by a summary in Section 5.

2. Observations and Data Analysis

ATCA Data:

The observations of the Galactic Centre were made at 3mm band with the ATCA between 2010 and 2014. ATCA is an array of six 22-m telescopes located at the Paul Wild Observatory in Narrabri, NSW, Australia. Of the six antennas, five have 3 mm receivers. The location of ATCA allows us to observe the GC for more than 8 hours a day, as the GC passes almost overhead at the latitude of ATCA. The Compact Array Broadband Backend (CABB) was upgraded in 2007. The upgrades allow us to make observations with two wide 2048 MHz intermediate frequency (IF) bands at the spectral resolution of 1 MHz, which corresponds to the velocity resolution of 3.5 km s^{-1} and the velocity coverage of ± 3500 km s^{-1}. This wide band makes it possible to detect several high velocity maser sources. We performed the observations in a spectral line mode wherein we observed at two different frequency bands centred at 86.243 and 85.640 GHz. These frequencies correspond to two transition lines of the SiO molecule ($J = 2 - 1$, $v = 1$ and $J = 2 - 1$, $v = 2$). Observations were performed for approximately $10 - 12$ hours each day. The bandpass calibration with PKS 1253 − 055 and flux calibration with Uranus were performed for 30 minutes each at the beginning and at the end of the observations, respectively. We observed the GC with three sets of 25 min on-source observations sandwiched between observations of gain calibrators (see Table 1). Sgr A* is a strong radio source thus it can be used for self calibration. These observations were carried out in part to study the variability of Sgr A* (see [62]). For the 3 mm observations, the maximum available baseline is 214 m for the H214 configuration which was the predominantly

Date	Array	Calibrators	Start Time		End Time	
			UT	JD	UT	JD
ATCA Observations						
2010 May 13	H214	1741-312	11:04:45	JD2455329.96042	21:50:25	JD2455330.41001
2010 May 14	H214	1622-297	10:45:07	JD2455330.948	22:07:40	JD2455331.42199
2010 May 15	H214	1741-312	10:10:30	JD2455331.92406	22:30:10	JD2455332.42406
2010 May 16	H214	1622-297	10:08:47	JD2455332.92277	21:35:60	JD2455333.41961
2011 May 23	H214	1741-312	09:57:43	JD2455704.91516	21:05:13	JD2455705.37862
2011 May 24	H214	1741-312	09:56:05	JD2455705.91395	21:24:17	JD2455706.39186
2011 May 25	H214	1741-312	10:01:13	JD2455706.91751	21:22:30	JD2455707.39062
2011 May 26	H214	1741-312	10:03:01	JD2455707.91876	21:17:33	JD2455708.38719
2012 May 15	H214	1714-336	08:23:47	JD2456062.84985	21:51:35	J2456063.41082D
2012 May 16	H214	1714-336	10:04:30	JD2456063.91979	21:45:22	J2456064.4065D
2012 May 17	H214	1714-336	09:49:17	JD2456064.90922	21:52:18	JD2456065.41132
2012 May 18	H214	1714-336	11:02:51	JD2456065.96031	21:56:46	JD2456066.41442
2013 June 26	EW352	1741-312	08:18:21	JD2456469.84608	20:44:37	JD2456470.36432
2013 June 27	EW 352	1741-312	—	—	—	—
2013 August 31	1.5A	1741-312	03:36:08	JD2456535.65009	14:57:04	JD2456536.12296
2013 September 1	1.5A	1741-312	—	—	—	—
2013 September 14	H214	1741-312	03:08:12	JD2456549.63069	13:27:588:12	JD2456549.63069
2013 September 16	H214	1741-312	—	—	—	—
2014 April 1	H168	1741-312	14:54:24	JD2456749.12111	23:38:55	JD2456749.48536
2014 April 2	H168	1741-312	13:37:58	JD2456750.06803	00:22:18	JD2456750.51549
2014 June 7	EW352	1714-336	08:00:50	JD2456815.83391	19:00:02	JD2456816.29169
2014 September 26	H214	1714-336	02:05:40	JD2456926.58727	12:44:31	JD2456927.03091
2014 September 27	H214	1714-336	02:10:13	JD2456927.59043	12:40:51	JD2456928.02837
ALMA Observation						
2015 April 15	C34-1/(2)	J1752-2956	06:16:33	JD2457122.761493	07:14:33	JD2457122.801771

Table 1: The Log of observations of Sgr A* taken using ATCA and ALMA. The dashes represent the days on which observations were not made. See Section 3 of [62] for details.

used configuration. This gives primary beam of $30''$ and synthesized beam of $1.99'' \times 2.28''$. The details of the observations are summarised in Table 1.

The MIRIAD data reduction package was used to map and reduce the interferometer data [63]. The bandpass, gain and flux calibrations were performed following the standard procedure. We then perform a hybrid Hogbom/Clark/Steer CLEAN algorithm to produce a clean map from a dirty map. The task UVLIN was used to separate the continuum from line in the spectral data using a linear fitting to the line-free channels and the output was subtracted from the calibrated data. The continuum-subtracted data were then mapped as a spectral cube. The typical rms noise in the individual channels is ~ 10 mJy.

ALMA Data:

We also use dataset that was observed using ALMA from the project 2013.1.00834.S (PI: J. Darling) and executed on 10 April 2015. The ALMA array was in C34-1/(2) configuration with 35 antennas of the main 12-m antenna array, and baselines ranging from 13 to 356 metres. The spectral setup consisted of 4 spectral windows with 1920 channels, centred at 85.321, 86.251,

87.181 and 88.11 GHz, with a bandwidth of 937.5 MHz and spectral resolution of 0.5 MHz which corresponds to the velocity resolution of $\sim$1.7 kms^{-1}. The configuration gives primary beam of 55″ and synthesized beam of $\sim 4.1 \times 2.5$ arcsec. The observations were made for 1 hour in total, starting with bandpass calibration with J1717 − 3342 and flux calibration with J1733 − 1304, and on source integration time of $\sim$ 38 minutes with phase calibration between on source observation.

Basic data reduction and standard calibration was performed using the Common Astronomy Software Application (CASA v4.2, [64]) with ALMA calibration pipeline. The continuum emission was subtracted from the calibrated data with a linear fitting to the line-free channels, and the spectral line map was produced using the CLEAN algorithm with natural weighting. The resulting image was corrected for primary beam to accurately represent the flux density of the detected sources. The obtained rms noise in the spectral channels is $\sim$ 2.5 mJy.

Further data analysis was performed using astropy [65] packages.

Detecting the SiO maser sources:

To detect SiO maser sources, first we calculated the rms noise σ for each channel after which, we searched for all the instances where the flux density was more than 5σ. These resulted in several candidate maser sources. We put additional constraints to distinguish the genuine sources from artifacts: the candidate should be detected over several epochs and over several channels. We detect the H42α recombination line (rest frequency= 85.69 GHz) in the ATCA data which is observed along the mini-spiral [66]. The detections from the recombination line have broad spectral width, and show extended features. These are excluded from the search of SiO maser candidate sources. We also referred to the lists of previously known stellar sources in the central parsec observed at 43 GHz and in IR observations [7, 51, 48] to verify the positions of detected candidates.

After this process, 5 sources were confirmed in the ATCA data and 20 sources in the ALMA data. The larger field-of-view and better sensitivity of ALMA facilitates the detection of weaker and greater number of sources further away from the centre. Of these, following are previously known sources: **ATCA data**: IRS 7, IRS 9, IRS 10EE, IRS 12N, and IRS 28; **ALMA data**: IRS 7, IRS 10EE, IRS 12N, IRS 14NE, IRS 15NE, IRS 17, IRS 19NW and IRS 28, and previously known 43 GHz SiO maser sources ([51, 48]) SiO 6, SiO 14, SiO 15, SiO 16, SiO 17, SiO 18, SiO 19, and SiO 20. Four new sources were also detected in the ALMA data, which have been observed for the first time in radio emission lines. Following the nomenclature used by [51] and [48], we have named them SiO 24, SiO 25, SiO 26 and SiO 27 (See Fig. 1).

3. Results

Proper Motion Analysis:

As discussed in Section 2, the longest baseline available for observation with ATCA is $\sim$ 214 m, and 356 m for the ALMA dataset, which translates to best possible angular resolution of $\sim 2''$. This is significantly lower resolution than the resolution available with VLBA at 43 GHz. To improve the accuracy in determination of the position of the source, we fit a two dimensional Gaussian to each detected source in each channel using DPUSER ([67]). We then obtain the position of the SiO maser for the observation day by weighted averaging the channel detections.

Source	Year	RA (″)	DEC (″)	Peak Jy
		ATCA Detections		
IRS 7	2010.364383	0.0580 ± 0.0365	5.3279 ± 0.0365	0.685 ± 0.032
	2010.367123	-0.0160 ± 0.0366	5.4459 ± 0.0365	0.788 ± 0.020
	2010.369863	0.0340 ± 0.0365	5.4019 ± 0.0365	0.654 ± 0.010
	2011.394520	-0.0960 ± 0.0368	5.3199 ± 0.0366	0.344 ± 0.028
	2011.397260	0.0920 ± 0.0368	5.3699 ± 0.0367	0.305 ± 0.022
	2011.400000	0.0860 ± 0.0366	5.4380 ± 0.0365	0.288 ± 0.024
	2012.372602	0.0320 ± 0.0323	5.5040 ± 0.0354	0.519 ± 0.022
	2012.375342	0.0180 ± 0.0316	5.3940 ± 0.0326	0.538 ± 0.023
	2012.378082	0.0599 ± 0.0318	5.5079 ± 0.0331	0.485 ± 0.022
	2012.380821	0.0159 ± 0.0326	5.4720 ± 0.0396	0.467 ± 0.022
	2014.252050	0.1639 ± 0.0316	5.3839 ± 0.0316	0.373 ± 0.037
	2014.432877	-0.1140 ± 0.0449	5.2339 ± 0.0749	0.400 ± 0.051
	2014.736986	-0.0800 ± 0.0316	5.3980 ± 0.0316	0.597 ± 0.023
	2014.739726	0.0840 ± 0.0316	5.4019 ± 0.0316	0.625 ± 0.047
IRS 9	2010.364383	5.6852 ± 0.0816	-6.3228 ± 0.0816	0.209 ± 0.024
	2010.367123	5.7602 ± 0.0817	-6.1762 ± 0.0816	0.226 ± 0.024
	2010.369863	5.6314 ± 0.0824	-6.1360 ± 0.0819	0.253 ± 0.026
	2011.394520	5.8888 ± 0.0840	-5.9422 ± 0.0824	0.243 ± 0.034
	2011.397260	5.7668 ± 0.0822	-6.0506 ± 0.0819	0.242 ± 0.023
	2011.400000	5.7024 ± 0.0817	-6.1248 ± 0.0817	0.299 ± 0.054
	2012.372602	5.6090 ± 0.0712	-6.2842 ± 0.0718	0.113 ± 0.024
	2012.375342	5.6382 ± 0.0765	-6.1046 ± 0.0883	0.121 ± 0.021
	2012.378082	5.5764 ± 0.0736	-6.0774 ± 0.0790	0.112 ± 0.026
	2012.380821	5.6736 ± 0.0709	-6.2280 ± 0.0732	0.139 ± 0.022
	2014.736986	5.8190 ± 0.1006	-6.1934 ± 0.1001	0.110 ± 0.023
	2014.739726	5.6662 ± 0.1008	-5.7426 ± 0.1007	0.146 ± 0.025
IRS 10EE	2010.364383	7.6720 ± 0.0817	4.0779 ± 0.0817	0.378 ± 0.021
	2010.367123	7.6776 ± 0.0816	4.2279 ± 0.0816	0.399 ± 0.022
	2010.369863	7.5818 ± 0.0816	4.1920 ± 0.0816	0.381 ± 0.021
	2011.394520	7.6126 ± 0.0817	4.1180 ± 0.0817	0.280 ± 0.024
	2011.397260	7.6018 ± 0.0818	4.1420 ± 0.0817	0.244 ± 0.020
	2011.400000	7.5806 ± 0.0818	4.1779 ± 0.0817	0.204 ± 0.018
	2012.372602	7.5163 ± 0.0720	3.8980 ± 0.0735	0.217 ± 0.017
	2012.375342	7.6503 ± 0.0750	4.2540 ± 0.0960	0.152 ± 0.013
	2012.378082	7.5348 ± 0.0723	4.4220 ± 0.0737	0.144 ± 0.015
	2012.380821	7.5770 ± 0.0750	3.9379 ± 0.0825	0.155 ± 0.014
	2014.249315	7.4437 ± 0.1415	3.8639 ± 0.1414	0.120 ± 0.010
IRS12N	2010.364383	-3.1940 ± 0.0824	-7.0684 ± 0.0820	0.100 ± 0.015
	2010.367123	-3.2439 ± 0.0820	-6.8922 ± 0.0819	0.143 ± 0.015
	2010.369863	-3.6560 ± 0.0820	-7.0163 ± 0.0818	0.160 ± 0.017
	2012.372602	-3.2560 ± 0.0579	-6.6343 ± 0.0583	0.260 ± 0.017
	2012.375342	-3.2959 ± 0.0578	-6.8578 ± 0.0583	0.223 ± 0.016
	2012.378082	-3.1279 ± 0.0578	-6.9894 ± 0.0581	0.200 ± 0.016
	2012.380821	-3.1100 ± 0.0624	-6.7728 ± 0.0723	0.230 ± 0.017
	2014.736986	-3.2500 ± 0.0817	-6.8633 ± 0.0816	0.480 ± 0.033
	2014.739726	-3.2960 ± 0.0818	-6.8612 ± 0.0817	0.490 ± 0.030

Table 2: Position offsets from Sgr A* and flux density of the detected SiO maser sources. '*' marks the newly discovered sources.

Source	Year	RA ($''$)	DEC ($''$)	Peak Jy
IRS 28	2010.364383	9.9878 ± 0.0828	-5.7386 ± 0.0820	0.134 ± 0.017
	2010.367123	10.3094 ± 0.0822	-5.7244 ± 0.0820	0.110 ± 0.014
	2010.369863	10.4244 ± 0.0817	-5.8432 ± 0.0817	0.153 ± 0.017
	2012.372602	10.4798 ± 0.0601	-5.8726 ± 0.0617	0.070 ± 0.015
	2012.375342	10.3314 ± 0.0633	-5.4248 ± 0.0763	0.074 ± 0.012
	2012.378082	10.3444 ± 0.0660	-6.1092 ± 0.0876	0.073 ± 0.012
	2012.380821	10.0470 ± 0.0644	-5.8776 ± 0.0766	0.065 ± 0.014
	2014.432877	10.2916 ± 0.0825	-5.8406 ± 0.0817	0.103 ± 0.018
	2014.736986	10.2344 ± 0.2097	-5.8964 ± 0.1725	0.100 ± 0.023
	2014.739726	10.0848 ± 0.0848	-5.9746 ± 0.0832	0.084 ± 0.015

ALMA Detections

Source	Year	RA ($''$)	DEC ($''$)	Peak Jy
IRS 7	2015.2726	0.0243 ± 0.0063	5.4330 ± 0.0039	0.494 ± 0.003
IRS 10EE	2015.2726	7.5930 ± 0.0110	4.0300 ± 0.0067	0.110 ± 0.003
IRS 12N	2015.2726	-3.3214 ± 0.0047	-7.0085 ± 0.0030	0.319 ± 0.003
IRS 14NE	2015.2726	0.6355 ± 0.0288	-8.2528 ± 0.0154	0.030 ± 0.003
IRS 15NE	2015.2726	1.0402 ± 0.0198	11.0842 ± 0.0127	0.082 ± 0.003
IRS 17	2015.2726	13.0620 ± 0.0128	5.4520 ± 0.0081	0.082 ± 0.003
IRS 19NW	2015.2726	14.3447 ± 0.0156	-18.5563 ± 0.0093	0.129 ± 0.003
IRS 28	2015.2726	10.4397 ± 0.0072	-5.8824 ± 0.0043	0.215 ± 0.003
SiO 6	2015.2726	35.0845 ± 0.0192	30.4963 ± 0.0114	0.336 ± 0.003
SiO 14	2015.2726	-7.5799 ± 0.0097	-28.5094 ± 0.0061	0.436 ± 0.003
SiO 15	2015.2726	-12.4102 ± 0.0146	-11.0621 ± 0.0096	0.094 ± 0.003
SiO 16	2015.2726	-26.4721 ± 0.0182	-34.4683 ± 0.0112	0.204 ± 0.003
SiO 17	2015.2726	7.9990 ± 0.0171	-27.7260 ± 0.0098	0.160 ± 0.003
SiO 18	2015.2726	-18.5807 ± 0.0224	-26.1446 ± 0.0138	0.102 ± 0.003
SiO 19	2015.2726	16.1361 ± 0.0112	-21.6761 ± 0.0070	0.165 ± 0.003
SiO 20	2015.2726	-13.9999 ± 0.0161	20.3122 ± 0.0101	0.094 ± 0.003
SiO 24*	2015.2726	17.0794 ± 0.0220	-9.2471 ± 0.0142	0.050 ± 0.003
SiO 25*	2015.2726	-33.1316 ± 0.0152	-17.9372 ± 0.0088	0.159 ± 0.003
SiO 26*	2015.2726	22.4607 ± 0.0302	23.5523 ± 0.0192	0.057 ± 0.003
SiO 27*	2015.2726	-20.3771 ± 0.0090	33.6992 ± 0.0201	0.106 ± 0.003

To calculate the proper motions of the masers, we assume that the stellar positions do not change within short time ($\sim$ days). We obtain the mean coordinates for a particular observation year by weighted averaging the positions obtained for each individual observation day. The 1σ uncertainty in the position measurement is obtained by following [68]. The weighted mean is given by $\bar{x} = \Sigma_i w_i x_x / \Sigma_i w_i$; $(i = 1, ..., n)$, where x_i are the position measurements, weights $w_i = 1/s_i^2$ and s_i are measurement uncertainties in x_i. The estimated error in the weighted mean is $\sigma = \sqrt{\sigma_1^2 + \sigma_2^2}$ where

$$\sigma_1 = \frac{1}{\sqrt{\Sigma_i w_i}}; \text{ and } \sigma_2 = \sqrt{\frac{\Sigma_i w_i (x_i - \bar{x})^2}{(n-1)\Sigma_i w_i}}$$

We then fit a weighted straight line through the resultant positions, along with the data from [51] and [48] to obtain the proper motions. We increased the uncertainties in the position values for large reduced χ^2 values. The detailed values of obtained positions of individual maser sources for
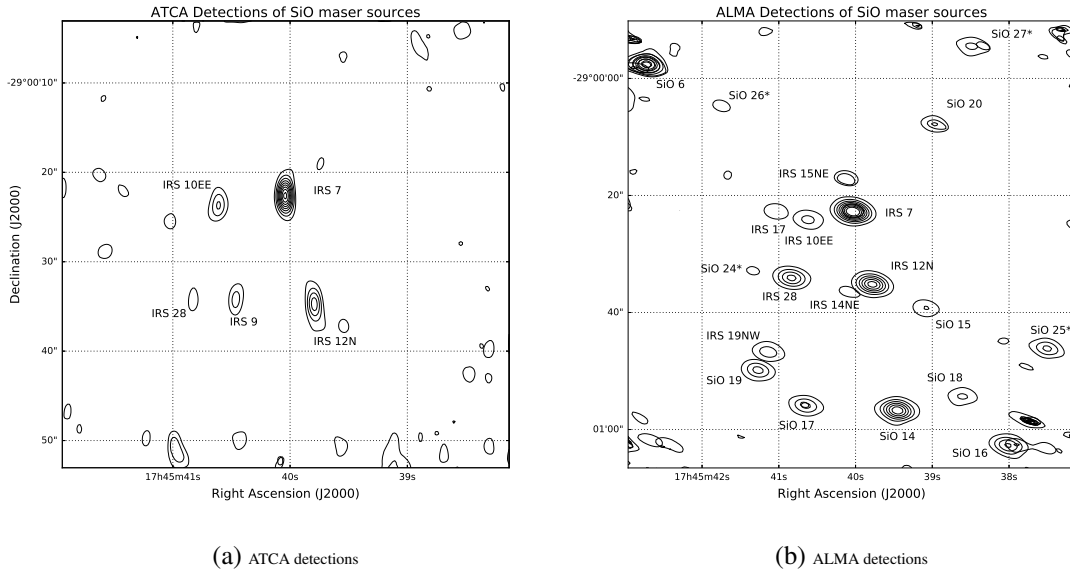
(a) ATCA detections   (b) ALMA detections

Figure 1: Positions of all the SiO maser sources detected with ATCA (*left*) and ALMA (*right*), respectively. Newly detected sources are marked with '*'. Contours are: *left*: 0.05, 0.093, 0.137, 0.18, 0.225,0.268, 0.312, 0.356, 0.4 Jy; *right*: 0.04, 0.09, 0.14, 0.19, 0.25, 0.29, 0.35, 0.4 Jy.

all epochs can be found in table 2. The scatter in the positions is consistent within the accuracy of angular resolution of $2''$ of our ATCA and ALMA observations.

Figure 2 shows the RA and DEC proper motions of the bright sources detected in the ATCA data with previously available data along with representative spectra from 17 December 2012. The red squares represent data from [51] and green diamonds represent data from [48], while the blue circles show points from our ATCA observations and the results from ALMA data are represented by the black triangles. The red dashed line in the images of spectra shows the 1σ rms noise. Figure 3 shows the proper motions of the sources detected from the ALMA dataset. The proper motion values are converted to linear velocities, where the distance to the GC is assumed to be 8 kpc. Table 3 shows the values of the linear speed of the maser sources. These proper motions are consistent within the error margin with the previous studies.

4. Discussion

In this section we discuss the properties of the individual detected SiO maser sources as inferred from the analysis of their spectra. The central stellar cluster of the GC has been observed at various wavelengths over several decades. The multiwavelength observations, especially in near-infrared (NIR) and mid-infrared (mid-IR) wavelength, have been used for not only determining the precise positions of the IR sources (IRSs), but they have also been used to infer their spectral energy distributions (SEDs), and from these, their morphology has been determined. Here we give a brief overview of these studies.
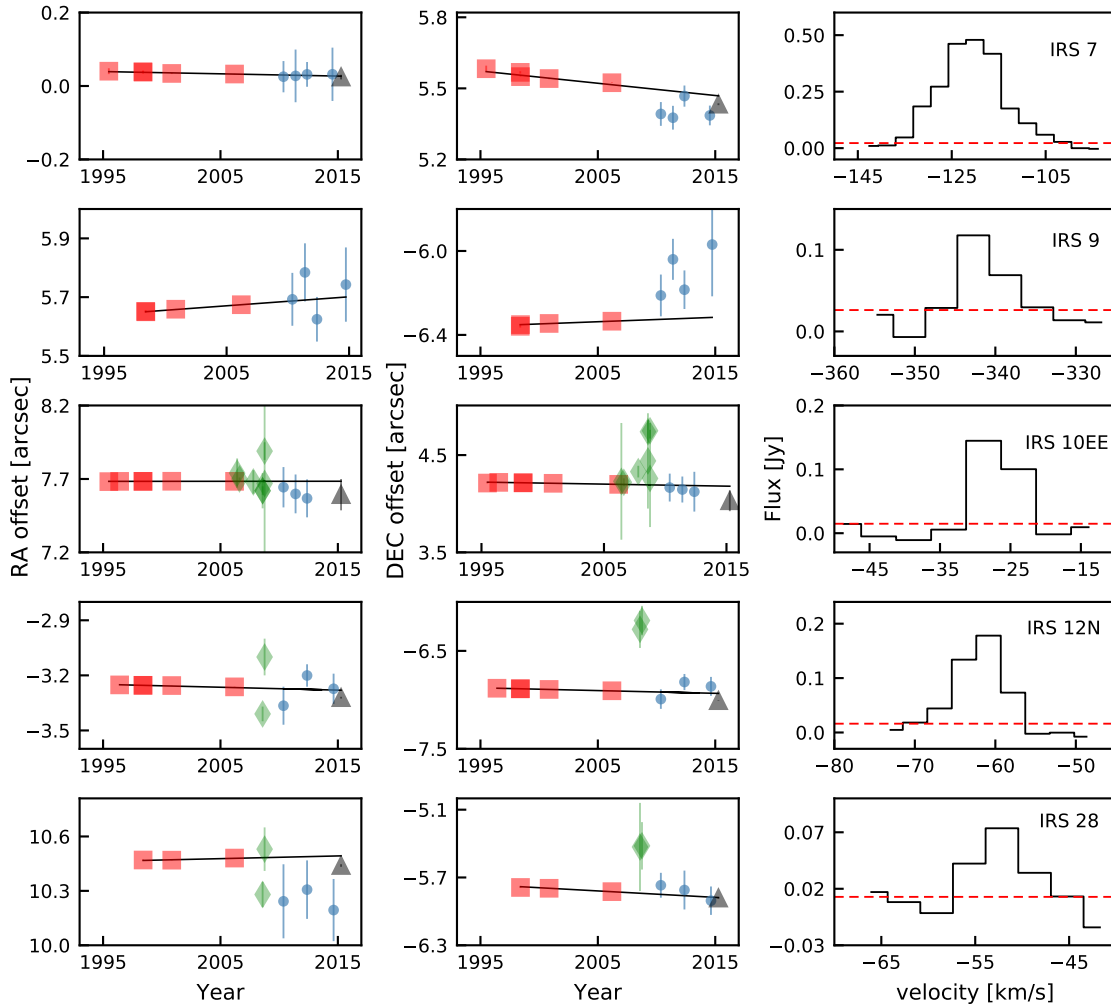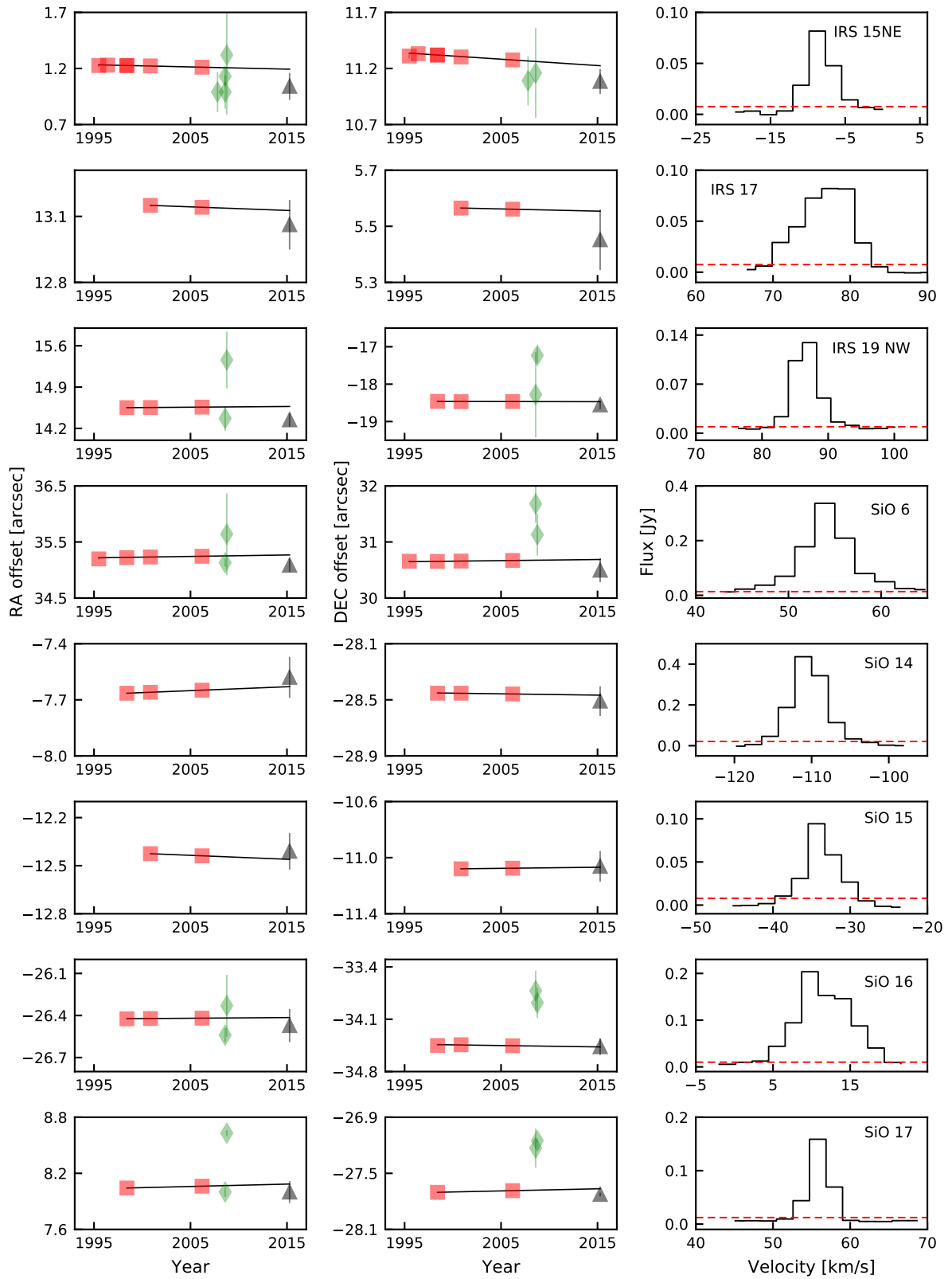
IRS 7:

Figure 2: The RA and DEC proper motion and the observed ATCA spectra of IRS 7, IRS 9, IRS 10EE, IRS 12N, and IRS 28. In the columns on left and centre, the data from [51] and [48] are represented by red squares and green diamonds, respectively. The blue circles represent data from our ATCA observations, and the results from ALMA data are represented by the black triangles. The red dashed line in right column shows the 1σ rms noise.

IRS 7 is a very strong radio SiO maser and IR source which has been used for adaptive optics guiding for IR observations. It is classified as M2 [69] or M1 [70] type red super giant with bright thermal radio emission from its external envelope. It has a supergiant luminosity with its SiO maser features spread over more than 20 km s^{-1}, which means that its envelope is much larger than typical Mira variable stars, with strongest features spanning about 10 mas. [70] detect a long period variability of 2620-2850 days and a shorter period of 470 ± 10 days. The detected variation in the flux of IRS 7 in our dataset is consistent with the latter.

IRS 9:

IRS 9 is a late-type giant [71] shown to have characteristics of a Mira variable star [51], of

Figure 3: The RA and DEC proper motion and the observed ATCA spectra of IRS 7, IRS 9, IRS 10EE, IRS 12N, and IRS 28. In the columns on left and centre, the data from [51] and [48] are represented by red squares and green diamonds, respectively. The blue circles represent data from our ATCA observations, and the results from ALMA data are represented by the black triangles. The red dashed line in right column shows the 1σ rms noise.
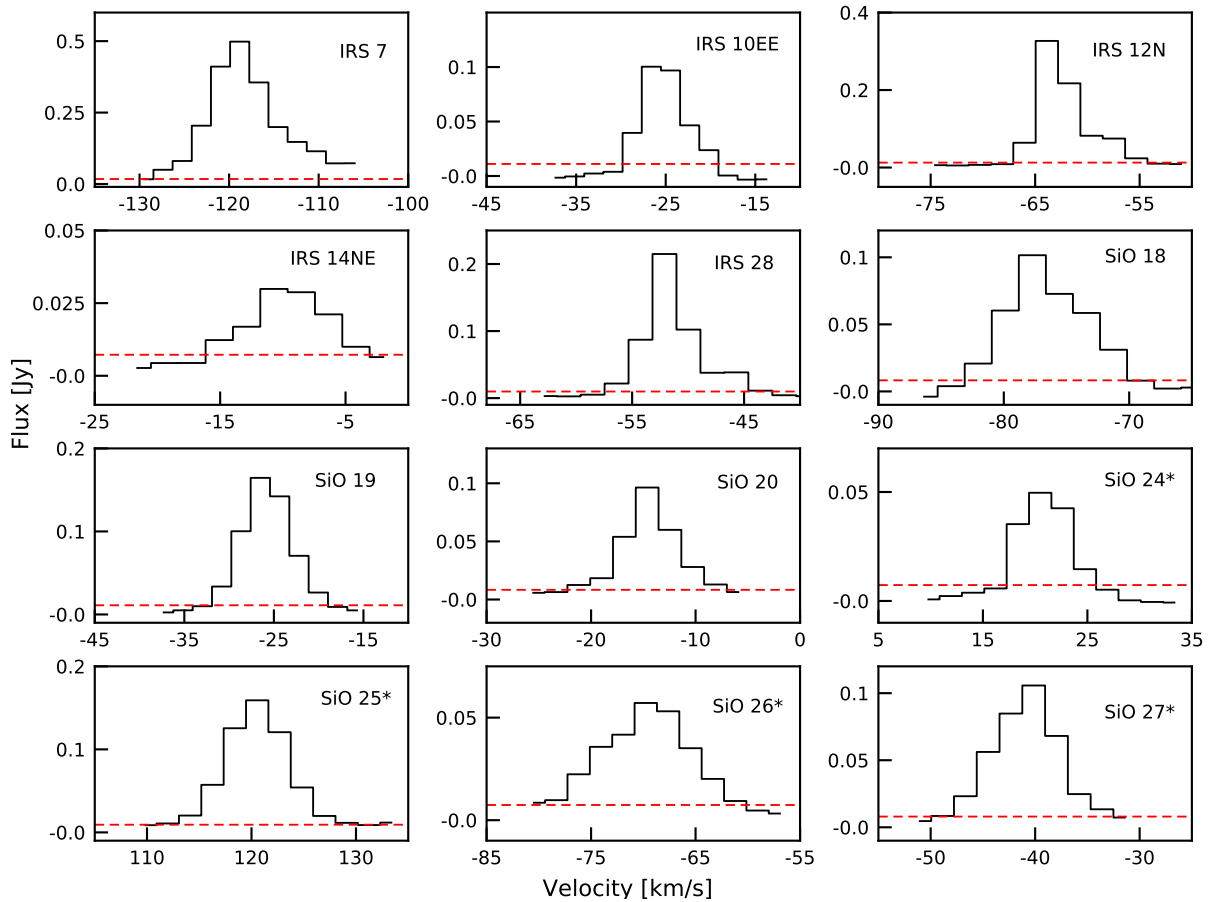
Figure 4: The spectra of the remaining sources detected with ALMA. The red dashed line shows the 1σ rms noise. The newly detected sources are marked with '*'

spectral type M3 III [72]. It exhibits a very high three-dimensional velocity, exceeding the escape velocity at its projected distance. A number of explanations were proposed (see [51] for detailed analysis) to explain the observed high velocity. A binary system was postulated to explain its high velocity, but [51] show that the contribution to the velocity from the binary could not be more than $20 \, \text{km s}^{-1}$, and thus it could not explain the high velocity. Other explanations included existence of $0.8 \times 10^6 \, M_\odot$ dark mass in the form of stellar remnants, the distance to the GC exceeding 9 kpc, a non-zero V_{LSR} of Sgr A*, or that IRS 9 is not bound to the GC. Their most-likely explanation is that it is a high-velocity star ejected from the central cluster. Calculations by [73] suggest that although IRS 9 has high velocity, it is not excessive with respect to the global distribution.

IRS 9 is known to have a long period variability [71]. [10] classify it to be large amplitude irregular or semi-regular variable, and [51] also consider it to be long period variable. In our ATCA data, it shows a variation in 86 GHz SiO emission over timescale of ~ 2 years, which is consistent with the long period variability. IRS 9 was not detected in the ALMA data, possibly due to contamination from the surrounding ISM.

IRS 10EE:

Source ID	V_{LSR} km/s	μ_{RA} mas/yr	μ_{DEC} mas/yr	V_{RA} km/s	V_{DEC} km/s
IRS7	-120 ± 4	-0.58 ± 0.10	-3.53 ± 0.41	-22.12 ± 3.9	-133.82 ± 15.4
IRS9	-340 ± 4	3.06 ± 0.07	2.11 ± 0.24	116.02 ± 2.6	80.10 ± 9.3
IRS10EE	-29 ± 4	0.03 ± 0.04	-2.09 ± 0.06	1.29 ± 1.6	-79.21 ± 2.2
IRS12N	-62 ± 4	-1.57 ± 0.27	-2.80 ± 0.48	-59.62 ± 10.1	-106.2 ± 18.1
IRS28	$+18 \pm 4$	1.49 ± 0.74	-5.71 ± 0.27	56.67 ± 28.1	-216.4 ± 10.4
IRS15NE	$+68 \pm 4$	-1.96 ± 0.06	-5.68 ± 0.11	-74.24 ± 2.2	-215.33 ± 4.1
IRS17	$+77 \pm 4$	-1.62 ± 0.14	-0.79 ± 0.27	-61.55 ± 5.4	-29.83 ± 10.2
IRS19NW	-53 ± 4	1.18 ± 0.22	-0.43 ± 0.28	44.97 ± 8.5	-16.31 ± 10.6
SiO6	$+43 \pm 4$	2.57 ± 0.39	1.97 ± 0.35	97.41 ± 14.9	74.88 ± 13.3
SiO14	-121 ± 4	2.08 ± 0.30	-0.94 ± 1.95	78.93 ± 11.5	-35.53 ± 73.9
SiO15	-44 ± 4	-2.46 ± 0.27	0.77 ± 0.52	-93.2 ± 10.1	29.29 ± 19.7
SiO16	$+1 \pm 4$	0.49 ± 0.07	-1.84 ± 1.08	18.65 ± 2.6	-69.62 ± 40.9
SiO17	$+47 \pm 4$	2.53 ± 0.07	2.25 ± 0.66	95.87 ± 2.8	85.55 ± 25.1

Table 3: SiO maser proper motions of the detected sources. The linear velocities are computed assuming 8 kpc distance to GC.

From the IR observations, IRS 10EE has been shown to be a long-period variable star, of spectral type M1 III Mira variable, with variability ranging from several days to few months [74, 75, 6, 10, 76]. It has also been observed at different maser lines, such as SiO, OH, and H_2O [77, 78, 49, 47, 50, 51, 59, 10]. The source also has a very compact SiO emission. It has been proposed that it could be a binary system [10], which has been supported by VLBA observations [59]. [48] detect variation on the timescale of months at 86 GHz. Since our observations are spaced every one year, this shorter variability cannot be detected in our data. We detect a steady decline in the peak flux density over the observation duration. [48] detect peak flux density between $0.24-0.45$ Jy at 86 GHz, which suggests a possibility of > 5 year long timescale variation.

IRS 12N:

IRS 12N has been observed in both IR and SiO line in radio, though it has a discrepancy between the IR and radio motions, possibly due to confusion caused by blending with other stars in the IR band. Similar to IRS 10EE, it has a very compact emission, and it has been classified as a cool red giant star [71, 7], possibly a M0 III type Mira variable star [72]. It shows a steady increase in the flux density in the ATCA data, but a decrease in the ALMA data suggesting a possible longer variability period. Similar longer timescale variation has been observed at 43 GHz by [51].

IRS 14NE:

IRS 14NE is an AGB star which has been observed in both IR and SiO line in radio and is often referred to as IRS 14N. It has been classified as M7 III type cool red giant [71] with possible long period variability (LPV) [79]. [72] classified it as M4 III late-type star. [6] and [10] find it to have a $K-$ band variability of ~ 0.14 magnitude and clear structure to the variability. Detected with a flux density of 30 mJy over only one spectral channel, IRS 14NE is the weakest SiO maser

source detected in our ALMA dataset.

IRS 15NE:

The observations of IRS 15NE have lent mixed identification results. It has been identified as cool AGB star by [80, 81] while [19], [8], and [82] classified it as WN9/Ofpe star. [79] found characteristic cool star features as well as strong He I and Brγ emission in the spectrum, suggesting that the IR spectrum could be blended with the emission from a massive hot star. [21] consider it to be a "transition" object, appearing as multiple sources. The 43 GHz VLBA observations by [59] observed slightly resolved SiO emission and the small maser emission size to be compatible with the AGB star classification. ATCA observations by [48] have shown that IRS 15NE is variable at both 43 and 86 GHz. It also exhibits high three-dimensional velocity.

IRS 17:

IRS 17 has been observed in both IR and radio line emission extensively over decades, and has been used to obtain accurate astrometry of the GC [50, 51, 83, 84, 85]. [86] and [87] classified it as a possible red supergiant and [86] found it to be bluer than IRS 7. It is classified as a late-type star by [88]. [79] consider it to be a possible LPV star.

IRS 19NW:

There have been very few observations of IRS 19NW in both IR and radio. It has been observed at 43 GHz by [50] and [51] with VLA and VLBA, and by [48] with ATCA, and in IR by [73] and [85]. IRS 19NW is one of the fainter sources in IR and is dominated by its bright neighbour IRS 19 [85].

IRS 28:

There have been several observations of IRS 28. [76] classified it as M6 III type red giant. [74] suggested that it is likely to be a variable while [71] classified it as LPV star. [10] find it to "not be clearly periodic", and rule out a period of $\sim$200 days observed by [89]. It is visible every other year in our dataset and shows a variation in flux from $\sim 110 - 150$ mJy in 2010 to ~ 70 mJy in 2012 to $\sim 85 - 100$ mJy in 2014, suggesting that it may have a long period of a couple of years. It also shows comparatively large three-dimensional velocity.

The 'SiO-' sources:

[51] and [48] have detected several new SiO maser sources at 43 GHz apart from the well known IR sources (IRSs), with a combined total of 23 new sources. These sources are not detected in our ATCA images. Some of the sources are outside the field of view, and thus are not observed. For the sources that are within the field of view, the peak flux densities at 43 GHz range from 0.015 Jy to ~ 0.1 Jy. Since the 43 GHz transition is usually (though not always) stronger than the 86 GHz transition [90], the corresponding peak flux density for these sources would be much lower at 86 GHz, where it would fall within $1 - 3\sigma$ of the rms noise, where $1\sigma = 0.015 - 0.030$ Jy. Thus most of these sources are not detected in our ATCA dataset. In the ALMA dataset, we identified 8 maser sources from the [51] and [48] 43 GHz datasets: *SiO-6, SiO 14, SiO 15, SiO 16, SiO 17, SiO 18, SiO 19*, and *SiO 20*. Four other sources were also observed, which represent new detections.

Following the nomenclature of [51] and [48], they were named as *SiO 24, SiO 25, SiO 26*, and *SiO 27*. Some of these sources have been previously observed at other wavelengths, though this is the first time they have been detected at mm wavelength. SiO 27 is a newly detected source which has not been observed at any other wavelengths. These newly detected sources are among the weaker sources detected in our ALMA data, with SiO 24, and SiO 26 having peak flux density ~ 50 mJy. Only IRS 14NE shows lower peak flux density.

SiO 6 has been identified with V4928 Sgr and PSD J174542.72-285957.4 [10] and is associated with OH, H_2O and SiO maser source OH 359.956-0.050 [91, 92, 93, 94]. A long period variable IRS 24 has been suggested as its IR counterpart [91, 71], although they are separated by large projected distance [10]. Analysis by [93] suggests that it is an evolved intermediate mass AGB star. [89] and [10] have observed large amplitude variability in the IR and is considered to be LPV candidate. [95] (*ID 11*) suggest it to have a variability on a yearly time scale.

SiO 16 is associated with V4911 Sgr, a LPV star [96]. It has been observed to have a period of ~ 528 days [89] while [10] found it to have irregular or semi-regular variability without signs of periodicity. [95] (*ID 451*) consider it to have a long period variability on yearly scale.

We identify **SiO 17** with OH 359.938-0.052 [94] which is a known OH/IR star. [95] (*ID 1933*) find it to be a non-variable star.

SiO 20 can be identified with PSD J174538.98-290007.7 from [10]. They observe a periodicity of ~ 325 days with large amplitude variations in both *H*- and *K*-bands, and consider it to be LPV star which is corroborated by [96] and [95] (*ID 1039*).

SiO 25 is associated with V4910 Sgr (PSD J174537.24-290045.7 of [10]) which is identified as a variable Star of Mira Cet type [96]. Similar to SiO 16, a long period of 601 days was observed by [89] but [10] found it to be irregular or semi-regular. A long timescale variability is detected by [95] (*ID 212*).

Several 'SiO-' sources have been discovered by [10], which are variable sources but do not show any periodicity. These are the following: **SiO 14** has been identified with PSD J174539.45-290056.6 [10] which is SSTGC 523553 from [96] and *ID 522* of [95]. [10] found it to be a blended star without any periodicity, but [71], [79], and [96] consider it to be late-type LPV star, and [95] also find a long timescale variability. **SiO 15** is considered to be PSD J174539.09-290039.3 [10], *ID 220* [95]. [71] consider it as a LPV candidate, and [95] find a yearly timescale variability. We identify **SiO 18** as PSD J174538.61-290054.3 [10]. It is classified as a late-type [88] and Mira-type long period variable star ([79, 95], *ID 552*). **SiO 19** is PSD J174541.27-290049.9 [10]. It has been identified as an AGB star [79] with a long yearly timescale variability [95], *ID 299*.

We identify **SiO 24** as PSD J174541.35-290033.0 [10], which is classified as a late-type star [88] with long timescale variability [95], *ID 778*. **SiO 26** is identified with PSD J174541.75-290004.6 [10]. [79] classified it as an AGB star. [96] and [95] (*ID 448*) consider it a LPV star. No counterpart was found for the star **SiO 27** in the literature, and represents a new detection.

Certain similarities can be observed in the detected sources in our datasets. These sources are predominantly late-type red supergiant and AGB stars, and have been observed at different wavelengths in millimetre line emission and IR. All sources detected in the ATCA dataset are classified as M-type variable stars and have negative LSR velocities. Most of the sources exhibit long period variability with a period of few months to few years. We do not detect any YSO candidates.

4.1 Variability of SiO masers

The SiO masers are associated with long period variable stars, such as AGB stars. They have been known to have variability of the timescale from few days to thousand days or more. The period of variability may not be strongly defined, and some times may be completely irregular. It is known that the SiO variability and the IR variability of a maser are correlated. The SiO and IR variabilities are related to the variation in the local heating rate due to underlying stellar pulsation, usually dominated by the radiative processes, where the IR stellar continuum radiation is absorbed by the SiO molecules in the circumstellar envelope [42, 97]. Our continuous monitoring of the GC allows us to study the variability of the SiO masers in the central parsec.

The detailed values of the flux densities observed - for each observation day when the source was detected - are given in table 2. The flux values are consistent within the measurement accuracy and rms noise for the same observation time ($\sim$ few days), but the values can be seen to vary significantly over longer periods. Some of the sources show a periodic behaviour while others show monotonic increase or decrease in the peak flux density. Sources such as IRS 7, IRS 9, and IRS 28 exhibit a variation timescale of the order of two years, IRS 10EE shows a gradual decrease in the peak flux density. The variation in the flux density of IRS 12N suggests a possibly longer period variability. Some of these sources are classified as Mira variable stars. Mira variable stars show strong variability of the order of few hundred days where their flux density in IR may change by more than a magnitude. Since the SiO variability is directly correlated with the IR variability, strong changes in the peak flux density are also expected at the SiO transition lines. Fig. 5 shows the flux density variation of the SiO maser sources seen in the ATCA and ALMA datasets over the period of the observations. Our conclusions on the variability of the sources are limited by our observation time of 5 years with an interval of $\sim$ 1 year. The weaker sources that exhibit a stable flux may have a weakly defined period on a different, possibly longer timescales than our observations, or their variability may be irregular.

5. Summary

We present our observations of the central parsec of the Galactic Centre with ATCA at 86 GHz, taken between 2010 and 2014. This is the largest dataset of GC observations at 3 mm wavelength. We detected 5 SiO maser sources, 4 have been reported at 3 mm for the first time viz. IRS 7, IRS 9, IRS 12N, and IRS 28. We also report the results from ALMA observation at 86 GHz taken on 10 April 2015. From this dataset, 20 sources were detected, of which 11 have been reported at 3 mm for the first time and 4 newly detected sources. We calculated the proper motion of these sources and the proper motion velocities are consistent with the previous observations within uncertainties. Our calculations of the proper motion though limited by resolution and sensitivity, are crucial for future high resolution and sensitivity observations and long term monitoring to constrain the proper motions of these sources and to get an insight into their orbits. We also studied the variability of the individual SiO maser sources. We detect significant variation in the flux density of the stars, though not all sources show a periodicity. We observe long period variability in the flux density of IRS 7, IRS 12N and IRS 28. Other sources show gradual increase or decrease, or irregular or weakly defined variation in the flux density.
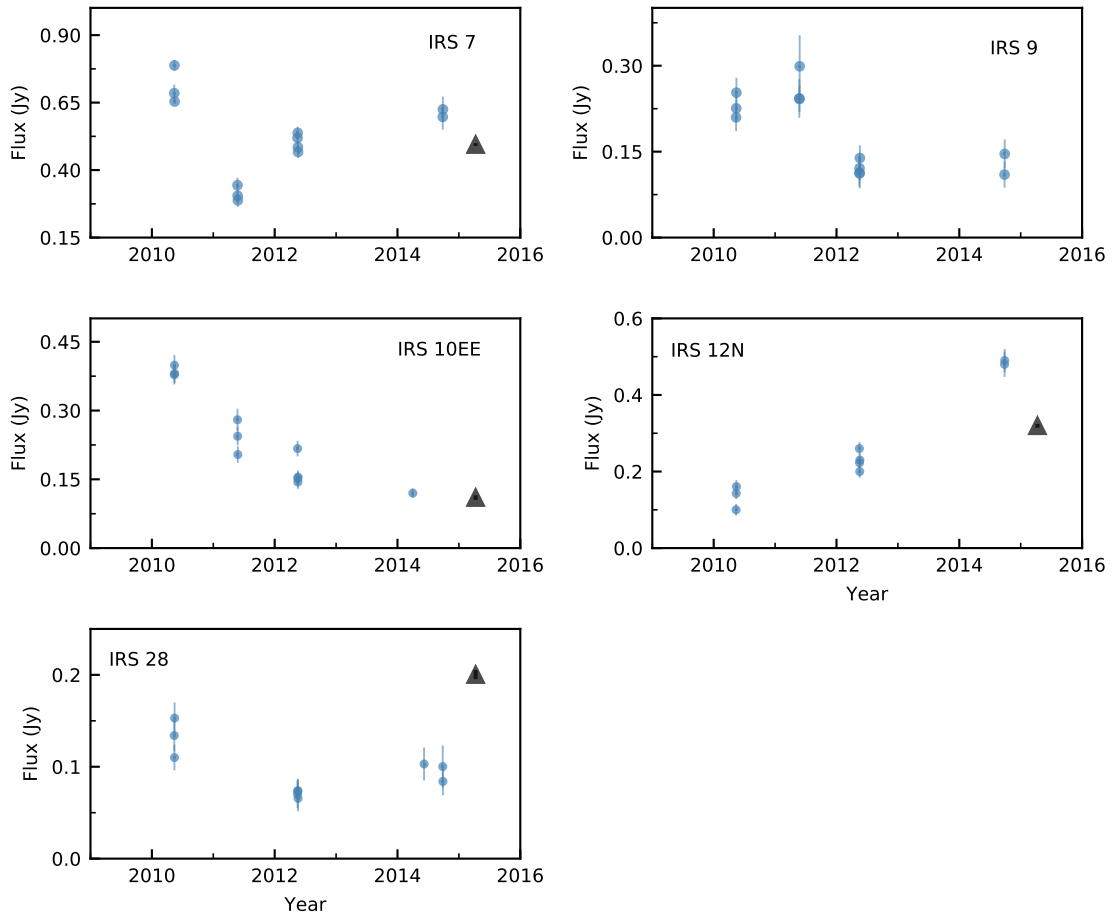
Figure 5: Observed variability in the peak flux of the SiO maser sources. The small blue circles represent the peak flux density observed in the ATCA dataset, while the peak flux density from the ALMA dataset is shown with black triangle. The error bars are 1σ rms noise in the channel in which the peak flux density is observed.

High resolution and high sensitivity observations at 3 mm wavelength, such as with the ALMA telescope and 3 mm-VLBI observations, would be crucial in the discovery of new and weaker sources in the 30 arcsec of Sgr A*, as well as in obtaining accurate proper motion of the stellar sources in the central parsec. Further observations in different frequency bands are necessary to obtain a census of the stars in central cluster, and to discover new AGB stars, red supergiants and YSOs in that region, which will help in improving our understanding of the nature of the central stellar disk.

Acknowledgements

References

[1] M. Morris and E. Serabyn, *The Galactic Center Environment*, *ARA&A* **34** (1996) 645.

[2] F. Melia and H. Falcke, *The Supermassive Black Hole at the Galactic Center*, *ARA&A* **39** (2001) 309 [`astro-ph/0106162`].

[3] M. J. Reid, *Is There a Supermassive Black Hole at the Center of the Milky Way?*, *International Journal of Modern Physics D* **18** (2009) 889 [`0808.2624`].

[4] R. Genzel, F. Eisenhauer and S. Gillessen, *The Galactic Center massive black hole and nuclear star cluster*, *Reviews of Modern Physics* **82** (2010) 3121 [`1006.0064`].

[5] A. Eckart, A. Hüttemann, C. Kiefer, S. Britzen, M. Zajaček, C. Lämmerzahl et al., *The Milky Way's Supermassive Black Hole: How Good a Case Is It?*, *Foundations of Physics* **47** (2017) 553 [`1703.09118`].

[6] T. Ott, A. Eckart and R. Genzel, *Variable and Embedded Stars in the Galactic Center*, *ApJ* **523** (1999) 248.

[7] T. Viehmann, A. Eckart, R. Schödel, J. Moultaka, C. Straubmeier and J.-U. Pott, *L- and M-band imaging observations of the Galactic Center region*, *A&A* **433** (2005) 117 [`astro-ph/0411798`].

[8] T. Paumard, R. Genzel, F. Martins, S. Nayakshin, A. M. Beloborodov, Y. Levin et al., *The Two Young Star Disks in the Central Parsec of the Galaxy: Properties, Dynamics, and Formation*, *ApJ* **643** (2006) 1011 [`astro-ph/0601268`].

[9] A. Tanner, D. F. Figer, F. Najarro, R. P. Kudritzki, D. Gilmore, M. Morris et al., *High Spectral Resolution Observations of the Massive Stars in the Galactic Center*, *ApJ* **641** (2006) 891 [`astro-ph/0510028`].

[10] M. S. Peeples, K. Z. Stanek and D. L. Depoy, *A Study of Stellar Photometric Variability Within the Central 4pc of the Galactic Center with Infrared Image Subtraction*, *ACTA Astronomica* **57** (2007) 173 [`astro-ph/0703769`].

[11] Y. Clénet, D. Rouan, E. Gendron, J. Montri, F. Rigaut, P. Léna et al., *Adaptive optics L-band observations of the Galactic Center region*, *A&A* **376** (2001) 124.

[12] A. Eckart, J. Moultaka, T. Viehmann, C. Straubmeier and N. Mouawad, *Young Stars at the Center of the Milky Way?*, *ApJ* **602** (2004) 760.

[13] J. Moultaka, A. Eckart, R. Schödel, T. Viehmann and F. Najarro, *VLT L-band mapping of the Galactic center IRS 3-IRS 13 region. Evidence for new Wolf-Rayet type stars*, *A&A* **443** (2005) 163 [`astro-ph/0507161`].

[14] T. Viehmann, A. Eckart, R. Schödel, J.-U. Pott and J. Moultaka, *Dusty Sources at the Galactic Center the N- and Q-Band Views with VISIR*, *ApJ* **642** (2006) 861 [`astro-ph/0601435`].

[15] D. A. Allen, A. R. Hyland and D. J. Hillier, *The source of luminosity at the Galactic Centre*, *MNRAS* **244** (1990) 706.

[16] A. Krabbe, R. Genzel, S. Drapatz and V. Rotaciuc, *A cluster of He I emission-line stars in the Galactic center*, *ApJ* **382** (1991) L19.

[17] R. D. Blum, D. L. Depoy and K. Sellgren, *A comparison of near-infrared spectra of the galactic center compact He I emission-line sources and early-type mass-losing stars*, *ApJ* **441** (1995) 603.

[18] R. D. Blum, K. Sellgren and D. L. Depoy, *Discovery of a possible Wolf-Rayet star at the galactic center*, *ApJ* **440** (1995) L17.

[19] A. Krabbe, R. Genzel, A. Eckart, F. Najarro, D. Lutz, M. Cameron et al., *The Nuclear Cluster of the Milky Way: Star Formation and Velocity Dispersion in the Central 0.5 Parsec*, *ApJ* **447** (1995) L95.

[20] P. Tamblyn, G. H. Rieke, M. M. Hanson, L. M. Close, D. W. McCarthy, Jr. and M. J. Rieke, *The Peculiar Population of Hot Stars at the Galactic Center*, *ApJ* **456** (1996) 206.

[21] F. Najarro, A. Krabbe, R. Genzel, D. Lutz, R. P. Kudritzki and D. J. Hillier, *Quantitative spectroscopy of the HeI cluster in the Galactic center.*, *A&A* **325** (1997) 700.

[22] A. M. Ghez, G. Duchêne, K. Matthews, S. D. Hornstein, A. Tanner, J. Larkin et al., *The First Measurement of Spectral Lines in a Short-Period Star Bound to the Galaxy's Central Black Hole: A Paradox of Youth*, *ApJ* **586** (2003) L127 [astro-ph/0302299].

[23] J. R. Lu, A. M. Ghez, S. D. Hornstein, M. R. Morris, E. E. Becklin and K. Matthews, *A Disk of Young Stars at the Galactic Center as Determined by Individual Stellar Orbits*, *ApJ* **690** (2009) 1463 [0808.3818].

[24] F. Yusef-Zadeh, M. Wardle, M. Sewilo, D. A. Roberts, I. Smith, R. Arendt et al., *Signatures of Young Star Formation Activity within Two Parsecs of Sgr A**, *ApJ* **808** (2015) 97 [1505.05177].

[25] A. Eckart, J. Moultaka, T. Viehmann, C. Straubmeier, N. Mouawad, R. Genzel et al., *New MIR Excess Sources north of the IRS 13 Complex*, *Astronomische Nachrichten Supplement* **324** (2003) 521.

[26] A. Eckart, R. Schödel, J. Moultaka, C. Straubmeier, T. Viehmann, S. Pfalzner et al., *The Galactic Center: The Stellar Cluster and the Massive Black Hole*, in *The Evolution of Starbursts*, S. Hüttmeister, E. Manthey, D. Bomans and K. Weis, eds., vol. 783 of *American Institute of Physics Conference Series*, pp. 17–25, Aug., 2005, DOI.

[27] A. Eckart, K. Mužić, S. Yazici, N. Sabha, B. Shahzamanian, G. Witzel et al., *Near-infrared proper motions and spectroscopy of infrared excess sources at the Galactic center*, *A&A* **551** (2013) A18 [1208.1907].

[28] K. Mužić, R. Schödel, A. Eckart, L. Meyer and A. Zensus, *IRS 13N: a new comoving group of sources at the Galactic center*, *A&A* **482** (2008) 173 [0802.4004].

[29] S. S. Kim and M. Morris, *Dynamical Friction on Star Clusters near the Galactic Center*, *ApJ* **597** (2003) 312 [astro-ph/0307271].

[30] S. F. Portegies Zwart, S. L. W. McMillan and O. Gerhard, *The Origin of IRS 16: Dynamically Driven In-Spiral of a Dense Star Cluster to the Galactic Center?*, *ApJ* **593** (2003) 352 [astro-ph/0303599].

[31] M. Wardle and F. Yusef-Zadeh, *On the Formation of Compact Stellar Disks around Sagittarius A**, *ApJ* **683** (2008) L37 [0805.3274].

[32] M. Mapelli, T. Hayfield, L. Mayer and J. Wadsley, *In Situ Formation of SgrA* Stars Via Disk Fragmentation: Parent Cloud Properties and Thermodynamics*, *ApJ* **749** (2012) 168 [`1202.0555`].

[33] B. Jalali, F. I. Pelupessy, A. Eckart, S. Portegies Zwart, N. Sabha, A. Borkar et al., *Star formation in the vicinity of nuclear black holes: young stellar objects close to Sgr A**, *MNRAS* **444** (2014) 1205 [`1408.0005`].

[34] D. F. Figer, *Massive Stars and The Creation of our Galactic Center*, *Astronomische Nachrichten Supplement* **324** (2003) 255 [`astro-ph/0207300`].

[35] A. Stolte, B. Hußmann, C. Olczak, W. Brandner, M. Habibi, A. M. Ghez et al., *Circumstellar discs in Galactic centre clusters: Disc-bearing B-type stars in the Quintuplet and Arches clusters*, *A&A* **578** (2015) A4 [`1502.03681`].

[36] L.-A. Nyman, P. J. Hall and H. Olofsson, *SiO masers in OH/IR stars, proto-planetary and planetary nebulae*, *A&AS* **127** (1998) 185.

[37] J. F. Desmurs, V. Bujarrabal, F. Colomer and J. Alcolea, *VLBA observations of SiO masers: arguments in favor of radiative pumping mechanisms*, *A&A* **360** (2000) 189 [`astro-ph/0006129`].

[38] P. J. Diamond and A. J. Kemball, *A Movie of a Star: Multiepoch Very Long Baseline Array Imaging of the SiO Masers toward the Mira Variable TX Cam*, *ApJ* **599** (2003) 1372 [`astro-ph/0310684`].

[39] W. D. Cotton, B. Mennesson, P. J. Diamond, G. Perrin, V. Coudé du Foresto, G. Chagnon et al., *VLBA observations of SiO masers towards Mira variable stars*, *A&A* **414** (2004) 275.

[40] M. D. Gray, M. Wittkowski, M. Scholz, E. M. L. Humphreys, K. Ohnaka and D. Boboltz, *SiO maser emission in Miras*, *MNRAS* **394** (2009) 51 [`0811.2770`].

[41] G. Perrin, W. D. Cotton, R. Millan-Gabet and B. Mennesson, *High-resolution IR and radio observations of AGB stars*, *A&A* **576** (2015) A70.

[42] M. Elitzur, *Astronomical masers*, *ARA&A* **30** (1992) 75.

[43] M. J. Reid, K. M. Menten, L. J. Greenhill and C. J. Chandler, *Imaging the Ionized Disk of the High-Mass Protostar Orion I*, *ApJ* **664** (2007) 950 [`0704.2309`].

[44] L. D. Matthews, L. J. Greenhill, C. Goddi, C. J. Chandler, E. M. L. Humphreys and M. W. Kunz, *A Feature Movie of SiO Emission 20-100 AU from the Massive Young Stellar Object Orion Source I*, *ApJ* **708** (2010) 80 [`0911.2473`].

[45] C. Goddi, E. M. L. Humphreys, L. J. Greenhill, C. J. Chandler and L. D. Matthews, *A Multi-epoch Study of the Radio Continuum Emission of Orion Source. I. Constraints on the Disk Evolution of a Massive YSO and the Dynamical History of Orion BN/KL*, *ApJ* **728** (2011) 15 [`1011.3799`].

[46] L. O. Sjouwerman, H. J. van Langevelde and P. J. Diamond, *Stellar positions from SiO masers in the Galactic center*, *A&A* **339** (1998) 897.

[47] L. O. Sjouwerman, M. Lindqvist, H. J. van Langevelde and P. J. Diamond, *H_2O and SiO maser emission in Galactic center OH/IR stars $O and SiO maser emission in Galactic center OH/IR stars*, *A&A* **391** (2002) 967.

[48] J. Li, T. An, Z.-Q. Shen and A. Miyazaki, *ATCA Observations of SiO Masers in the Galactic Center*, *ApJ* **720** (2010) L56.

[49] K. M. Menten, M. J. Reid, A. Eckart and R. Genzel, *The Position of Sagittarius A*: Accurate Alignment of the Radio and Infrared Reference Frames at the Galactic Center*, *ApJ* **475** (1997) L111.

[50] M. J. Reid, K. M. Menten, R. Genzel, T. Ott, R. Schödel and A. Eckart, *The Position of Sagittarius A*. II. Accurate Positions and Proper Motions of Stellar SiO Masers near the Galactic Center*, *ApJ* **587** (2003) 208 [`astro-ph/0212273`].

[51] M. J. Reid, K. M. Menten, S. Trippe, T. Ott and R. Genzel, *The Position of Sagittarius A*. III. Motion of the Stellar Cusp*, *ApJ* **659** (2007) 378 [`astro-ph/0612164`].

[52] H. Izumiura, S. Deguchi and T. Fujii, *SiO Maser Forest at the Galactic Center*, *ApJ* **494** (1998) L89 [`astro-ph/9712101`].

[53] A. Miyazaki, S. Deguchi, M. Tsuboi, T. Kasuga and S. Takano, *SiO Maser Survey in the Galactic Center Region with a Multi-Beam Receiver*, *PASJ* **53** (2001) 501.

[54] S. Deguchi, T. Fujii, H. Izumiura, O. Kameya, Y. Nakada, J.-i. Nakashima et al., *SiO Maser Survey of the Galactic Disk IRAS Sources. II., the Galactic Center Area*, *ApJS* **128** (2000) 571.

[55] S. Deguchi, T. Fujii, H. Izumiura, O. Kameya, Y. Nakada and J.-i. Nakashima, *SIO Maser Survey of the Galactic Disk IRAS Sources. III., a Central Part of the Galaxy*, *ApJS* **130** (2000) 351.

[56] S. Deguchi, T. Fujii, J.-I. Nakashima and P. R. Wood, *Near-Infrared Observations of the IRAS/SiO Sources in the Galactic Bulge: a Large Scale Distribution*, *PASJ* **54** (2002) 719.

[57] L. O. Sjouwerman, M. Messineo and H. J. Habing, *43 GHz SiO Masers and Astrometry with VERA in the Galactic Center*, *PASJ* **56** (2004) 45.

[58] H. Imai, S. Deguchi, T. Fujii, I. S. Glass, Y. Ita, H. Izumiura et al., *Detections of SiO Masers from the Large-Amplitude Variables in the Galactic Nuclear Disk*, *PASJ* **54** (2002) L19 [`astro-ph/0204110`].

[59] T. Oyama, M. Miyoshi, S. Deguchi, H. Imai and Z.-Q. Shen, *A Measurement of Proper Motions of SiO Maser Sources in the Galactic Center with the VLBA*, *PASJ* **60** (2008) 11 [`0710.1393`].

[60] M. Lindqvist, N. Ukita, A. Winnberg and L. E. B. Johansson, *SiO maser emission from OH/IR stars close to the Galactic centre*, *A&A* **250** (1991) 431.

[61] M. Messineo, H. J. Habing, L. O. Sjouwerman, A. Omont and K. M. Menten, *86 GHz SiO maser survey of late-type stars in the Inner Galaxy. I. Observational data*, *A&A* **393** (2002) 115 [`astro-ph/0207284`].

[62] A. Borkar, A. Eckart, C. Straubmeier, D. Kunneriath, B. Jalali, N. Sabha et al., *Monitoring the Galactic Centre with the Australia Telescope Compact Array*, *MNRAS* **458** (2016) 2336 [`1605.00424`].

[63] R. J. Sault, P. J. Teuben and M. C. H. Wright, *A Retrospective View of MIRIAD*, in *Astronomical Data Analysis Software and Systems IV*, R. A. Shaw, H. E. Payne and J. J. E. Hayes, eds., vol. 77 of *Astronomical Society of the Pacific Conference Series*, p. 433, 1995, `astro-ph/0612759`.

[64] J. P. McMullin, B. Waters, D. Schiebel, W. Young and K. Golap, *CASA Architecture and Applications*, in *Astronomical Data Analysis Software and Systems XVI*, R. A. Shaw, F. Hill and D. J. Bell, eds., vol. 376 of *Astronomical Society of the Pacific Conference Series*, p. 127, Oct., 2007.

[65] Astropy Collaboration, T. P. Robitaille, E. J. Tollerud, P. Greenfield, M. Droettboom, E. Bray et al., *Astropy: A community Python package for astronomy*, *A&A* **558** (2013) A33 [`1307.6212`].

[66] P. A. Jones, M. G. Burton, M. R. Cunningham, M. A. Requena-Torres, K. M. Menten, P. Schilke et al., *Spectral imaging of the Central Molecular Zone in multiple 3-mm molecular lines*, *MNRAS* **419** (2012) 2961 [`1110.1421`].

[67] T. Ott, "DPUSER: Interactive language for image analysis." Astrophysics Source Code Library, Mar., 2013.

[68] Z. M. Malkin, *On the calculation of mean-weighted value in astronomy*, *Astronomy Reports* **57** (2013) 882.

[69] M. Perger, J. Moultaka, A. Eckart, T. Viehmann, R. Schödel and K. Muzic, *Compact mid-IR sources east of Galactic Center source IRS5*, *A&A* **478** (2008) 127.

[70] T. Paumard, O. Pfuhl, F. Martins, P. Kervella, T. Ott, J.-U. Pott et al., *<ASTROBJ>GCIRS 7</ASTROBJ>, a pulsating M1 supergiant at the Galactic centre . Physical properties and age*, *A&A* **568** (2014) A85 [1406.5320].

[71] R. D. Blum, K. Sellgren and D. L. Depoy, *JHKL Photometry and the K-Band Luminosity Function at the Galactic Center*, *ApJ* **470** (1996) 864 [astro-ph/9604109].

[72] D. F. Figer, D. Gilmore, S. S. Kim, M. Morris, E. E. Becklin, I. S. McLean et al., *High-Precision Stellar Radial Velocities in the Galactic Center*, *ApJ* **599** (2003) 1139 [astro-ph/0309210].

[73] S. Trippe, S. Gillessen, O. E. Gerhard, H. Bartko, T. K. Fritz, H. L. Maness et al., *Kinematics of the old stellar population at the Galactic centre*, *A&A* **492** (2008) 419 [0810.1040].

[74] M. Tamura, M. W. Werner, E. E. Becklin and E. S. Phinney, *Detection of Stellar Variability in the Central Parsec of the Galaxy*, *ApJ* **467** (1996) 645.

[75] P. R. Wood, H. J. Habing and P. J. McGregor, *Infrared monitoring of OH/IR stars near the Galactic Center*, *A&A* **336** (1998) 925.

[76] Q. Zhu, R. P. Kudritzki, D. F. Figer, F. Najarro and D. Merritt, *Radial Velocities of Stars in the Galactic Center*, *ApJ* **681** (2008) 1254 [0803.1826].

[77] M. Lindqvist, A. Winnberg and J. R. Forster, *Water vapour masers in envelopes of OH/IR stars close to the Galactic centre*, *A&A* **229** (1990) 165.

[78] M. Lindqvist, A. Winnberg, H. J. Habing and H. E. Matthews, *OH/IR stars close to the Galactic Centre. I - Observational data*, *A&AS* **92** (1992) 43.

[79] R. D. Blum, S. V. Ramírez, K. Sellgren and K. Olsen, *Really Cool Stars and the Star Formation History at the Galactic Center*, *ApJ* **597** (2003) 323 [astro-ph/0307291].

[80] R. Genzel, N. Thatte, A. Krabbe, H. Kroker and L. E. Tacconi-Garman, *The Dark Mass Concentration in the Central Parsec of the Milky Way*, *ApJ* **472** (1996) 153.

[81] R. Genzel, C. Pichon, A. Eckart, O. E. Gerhard and T. Ott, *Stellar dynamics in the Galactic Centre: proper motions and anisotropy*, *MNRAS* **317** (2000) 348 [astro-ph/0001428].

[82] F. Martins, R. Genzel, D. J. Hillier, F. Eisenhauer, T. Paumard, S. Gillessen et al., *Stellar and wind properties of massive stars in the central parsec of the Galaxy*, *A&A* **468** (2007) 233 [astro-ph/0703211].

[83] R. Schödel, D. Merritt and A. Eckart, *The nuclear star cluster of the Milky Way: proper motions and mass*, *A&A* **502** (2009) 91 [0902.3892].

[84] S. Gillessen, F. Eisenhauer, S. Trippe, T. Alexander, R. Genzel, F. Martins et al., *Monitoring Stellar Orbits Around the Massive Black Hole in the Galactic Center*, *ApJ* **692** (2009) 1075 [0810.4674].

[85] P. M. Plewa, S. Gillessen, F. Eisenhauer, T. Ott, O. Pfuhl, E. George et al., *Pinpointing the near-infrared location of Sgr A* by correcting optical distortion in the NACO imager*, *MNRAS* **453** (2015) 3234 [1509.01941].

[86] G. H. Rieke, C. M. Telesco and D. A. Harper, *The infrared emission of the Galactic center*, *ApJ* **220** (1978) 556.

[87] M. J. Lebofsky, G. H. Rieke, M. R. Deshpande and J. C. Kemp, *Polarization of compact sources in the galactic center*, *ApJ* **263** (1982) 672.

[88] A. Feldmeier-Krause, W. Kerzendorf, N. Neumayer, R. Schödel, F. Nogueras-Lara, T. Do et al., *KMOS view of the Galactic Centre - II. Metallicity distribution of late-type stars*, *MNRAS* **464** (2017) 194 [1610.01623].

[89] I. S. Glass, S. Matsumoto, B. S. Carter and K. Sekiguchi, *Large-amplitude variables near the Galactic Centre*, *MNRAS* **321** (2001) 77.

[90] L.-A. Nyman, P. J. Hall and T. Le Bertre, *Infrared and SiO maser observations of OH/IR stars*, *A&A* **280** (1993) 551.

[91] D. A. Levine, D. F. Figer, M. Morris and I. S. McLean, *A Circumstellar H 2O Maser Associated with the Circumnuclear Molecular Disk at the Galactic Center?*, *ApJ* **447** (1995) L101.

[92] F. Yusef-Zadeh and D. M. Mehringer, *An H 2O Maser near Sagittarius A East: Evidence for Active Massive Star Formation near the Galactic Center*, *ApJ* **452** (1995) L37.

[93] L. O. Sjouwerman and H. J. van Langevelde, *OH Counterparts for H 2O Masers in the Galactic Center: Evolved Stars instead of Signs of Recent Star Formation*, *ApJ* **461** (1996) L41.

[94] L. O. Sjouwerman, H. J. van Langevelde, A. Winnberg and H. J. Habing, *A new sample of OH/IR stars in the Galactic center*, *A&AS* **128** (1998) 35.

[95] H. Dong, R. Schödel, B. F. Williams, F. Nogueras-Lara, E. Gallego-Cano, T. Gallego-Calvente et al., *Near-infrared variability study of the central 2.3 arcmin × 2.3 arcmin of the Galactic Centre - I. Catalogue of variable sources*, *MNRAS* **470** (2017) 3427 [1706.03243].

[96] N. Matsunaga, T. Kawadu, S. Nishiyama, T. Nagayama, H. Hatano, M. Tamura et al., *A near-infrared survey of Miras and the distance to the Galactic Centre*, *MNRAS* **399** (2009) 1709 [0907.2761].

[97] J. R. Pardo, J. Alcolea, V. Bujarrabal, F. Colomer, A. del Romero and P. de Vicente, ^{28}*SiO v = 1 and v = 2, J = 1-0 maser variability in evolved stars. Eleven years of short spaced monitoring*, *A&A* **424** (2004) 145.